International Journal of Fracture **97:** 321–336, 1999.

On damage distribution in the upsetting process of sintered porous materials

A. SHIRIZLY[1], D. RITTEL[2], L. RUBINSKI[2] and J. TIROSH[2]
[1]*University of Waterloo, Faculty of Mechanical Engineering, N2L 3G1 Waterloo, Ontario, Canada.*
e-mail: shirizly@mechanical.watstar.uwaterloo.ca
[2]*Faculty of Mechanical Engineering, Technion, Haifa 32000, Israel*

Received 24 March 1997; accepted in revised form 21 November 1997

Abstract. The common information about the *average* porosity of a given porous material (like sintered powder materials) may not be sufficient for design purposes. It is evident that an occasional localization of pores ('damage') may trigger premature failure at a low global average porosity. In order to avoid this limitation we suggest here two measuring techniques to assess the spatial distribution of the damage in one and two dimensions. (1) *Macro-measurement*: The idea is based on removing (in consecutive steps) thin layers from the outer boundary of the workpiece and measuring the density and weight of the residual workpiece between each step. The repeated cycles of 'cutting and measuring' give the distribution of the pores in the cross section of the workpiece (averaged across the height of the section). (2) *Micro-measurement*: Magnified pictures are taken from selected metallographic sections of the workpiece. An area scanner is employed to measure the 'local porosity' by providing the ratio between the dark areas to the total area occupied by each picture. This procedure renders directly the 2D distribution of the pores in a given cross section. Porous specimens made by powder metallurgy (Fe and 304 stainless steel) are compressed unidirectionally. The evolution of the porosity due to the compacting process is measured by these two techniques. The measurements show how the initial pore distribution evolves in space and time during the compression process. The results are compared to a semi-analytical simulation of the densification process using the limit analysis formulations.

Key words: Damage distribution, upsetting, porous materials, density.

1. Introduction

Damage distribution in sintered materials (e.g. pores, cavities) is known to influence their flow properties. Even in virgin materials, the distribution of pores is not uniform, as shown for example in Figure 1. The scattering of the nonuniformities may vary after a certain amount of plastic deformation. The need to provide a *measured information on such evolution* seems mandatory for reliable modeling of the material.

Wray et al. (1983) and Spitzig et al. (1985) used the Dirichlet cell analysis in order to find the local area fraction of pores in different Fe compacts. They found large variation of the local porosity with respect to the average (planar) porosity (4–7 times). They also reported good agreement between the planar and bulk porosity of their material. Schneider et al. (1996) used automated image analysis and reported similar results for iron powder. Moon and Yang (1992) proposed a method of measurement for the determination of the relative density in axisymmetric forming of sintered porous material. Their experimental technique relies on the grid patterns of the deformed specimen.

The theoretical modeling of porous materials was carried out earlier by Gurson (1977) who proposed a proper plastic potential from which the constitutive response is derived. Some modifications were later proposed to account for actual material behavior, for example, by Spitzig et al. (1988); Wang et al. (1990; 1992); Tvergaard (1981; 1982); Hagai and Anand

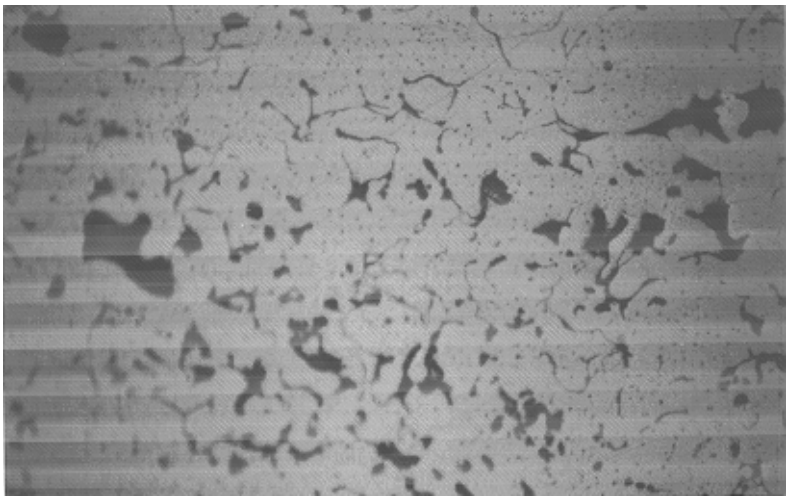

Figure 1. Micrograph showing the pore structures in sintered powder materials (Fe with relative porosity of 0.28).

(1993). In the spirit of Gurson's model, their analysis gave an *integrated* response of the bulk behavior rather than a *local* response. This lack of local information motivated recently a limit analysis study of porous media with an intention to incorporate the spatial distribution of the porosity throughout the governing formulation (Shirizly et al., 1996). The data to which the analysis was compared (taken from the open literature) were *averaged values* and thus insufficient for engineering purposes. In this paper, we extend our approach by characterizing actual materials and introduce two measuring techniques in order to assess the evolution of the density and the pores (damages) distribution compared with the analytical solution.

2. Basic notions in porous continua

Two new scalar variables are seemingly essential in describing the constitutive behavior of porous materials which do not appear in the classical theories of plasticity: The distribution of the porosity $f(x_i)$ and the distribution of the hydrostatic pressure $\Sigma_{kk}(x_i)$ in the volume of the material defined by the spatial coordinates x_i. The widely used yield function Φ which incorporates these two variables (albeit in an average form) was suggested by Gurson (1977) who was motivated by the micro mechanics of void growth. This model is relatively convenient for engineering applications due to the ease by which one can attribute physical meaning to the two mentioned variables. It is given below with two modifications (suggested by Wang et al., 1990; 1992)

$$\Phi = \frac{\frac{3}{2}\Sigma'_{ij}\Sigma'_{ij}}{\bar{\sigma}^2} + 2q_1 f^N \cosh\left(\frac{N}{2} q_2 \frac{\Sigma_{kk}}{\bar{\sigma}}\right) - [1 + q_3 f^{2N}], \tag{1}$$

where Σ_{kk} is the first invariant of the macroscopic Cauchy stress tensor; Σ'_{ij} is the macroscopic deviatior stress tensor; f is the current void fraction; q_1, q_2 and q_3 scalars; and $\bar{\sigma}$ is the effective stress of the matrix material, defined by

$$\bar{\sigma} = \sqrt{\tfrac{3}{2}\sigma'_{ij}\sigma'_{ij}} \quad \text{and} \quad \bar{\sigma} = k_0 \bar{\varepsilon}^n \quad (0 \leqslant n \leqslant 1), \tag{2}$$

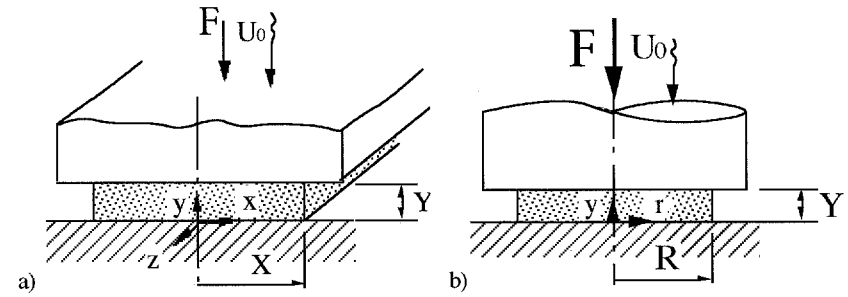

Figure 2. Schematic view of the forged specimens made from a sintered powder material (a) long bar compression; (b) circular disk compression.

where σ'_{ij} is the matrix local stress deviator. $\bar{\varepsilon}$ is the equivalent strain of the matrix material (conjugate to $\bar{\sigma}$). k_0 is a material constant and n is its strain hardening exponent.

Tvergaard (1981; 1982) added into Equation (1) the scalars q_1, q_2 and q_3 (which are otherwise unity) to soften the effect of the hydrostatic stress on the deformation rates. Wang et al. (1990; 1992) added the exponent N to the void fraction, f, in (1) to moderate somewhat the effect of the porosity on the deformation rates, as follows

$$N = \frac{2+n}{3} \quad \text{for } 0 \leqslant n \leqslant 1 \quad (n \text{ is the strain hardening exponent}); \tag{3}$$

so that N varies between $\frac{2}{3}$ *to* 1 in nonhardening $(n = 0)$ and linear hardening $(n = 1)$ matrix material respectively. In the special case of $q_1 = q_2 = q_3 = N = 1$, (1) reduces to the original Gurson's equation.

3. An outline of the solution

The solution to which the forthcoming measurements are compared is based on the limit analysis procedures (upper and lower bounds) described in details elsewhere (Shirizly et al., 1996). Briefly described, an admissible velocity field for the bulk material is assumed and used to find the material constitutive response to the compressive load. Concurrently, an admissible yielding stress field is employed to assess the effect of the hydrostatic stress on the bulk flow. The combination of the these two admissible fields is used in the upper bound formulation modified to account for the overall material compressibility (Tirosh and Iddan, 1989). The outcome provides an engineering tool to predict, with a certain degree of approximation, the required load to densify the porous material. The advantage of such an analysis is that the results are independent *of the actual mechanism by which the compacting process is evolved.* The basic algorithm is recapitulated in Appendix I. The solution is compared to experiments in different geometries: (a) upsetting of long bars and (b) upsetting of circular discs. They are shown in Figure 2.

4. The measuring techniques

The load required to densify porous material is an average value which does not discriminate between uniform and non-uniform distribution of the pores. Therefore, the two measuring techniques described below are developed to provide a measured information of the pore distribution.

The two forming processes (shown in Figure 2) are considered in details: plain strain (long bar) and axisymmetric (circular disk). In both cases, the porous specimens are deformed plastically by an external unknown load **F** which moves downward at a prescribed speed U_0. The initial and subsequent pore distribution in the workpiece are determined by the following procedures.

4.1. THE MACROSCOPIC MEASUREMENT

The technique is based on cutting thin layers from the outer boundary of the workpiece (at consecutive steps of the process) and measuring the current weight and density of the residual workpiece between steps as shown in Figures 3a and 3b. The (unidirectional) distribution of porosity ρ (i.e., $\rho(x)$ for plain strain and $\rho(r)$ for axisymmetric compression) is assessed by repeated cycles of 'cutting and measuring'. However, the density distribution is still averaged across the height of the cut. The weighting of the residual specimen after each step (by soaking in water, etc. according to ASTM standard (B311-86)) needs a special refinement to take into account the various possible pore morphologies. According to their location in the specimen, pores can be either open, closed or ill-defined, as shown schematically in Figure 4a. The complexity in defining the material water-free volume in the actual material is shown in Figures 4b and 4c.

When the specimen is soaked into the distilled water, a certain amount of water may penetrate into the open pores and bias the true weight. In order to prevent the pore/water interaction a very thin plastic cover is heat stretched around the specimen to seal against penetration of the water (a low density polyethylene cover with density of 0.919 gr/cm^3 and thickness less than 0.014 mm before the stretch operation). The covering procedure was carried out carefully to minimize the possibility of trapped air bubbles between the covering sheet and the specimen. The experimental error induced by this phenomenon, if at all, is believed to be negligible.

To determine the porosity level in the incremental sliced layer $D_R(x)$, it is necessary to solve the volume and mass conservation equations. The density $D_R(x)$, is obtained by

$$D_R(x) = D_B \frac{\frac{W_T}{W_B} - 1}{\frac{W_T}{W_B}\frac{D_B}{D_T} - 1}, \tag{4}$$

where, W_T, W_B and W_R are the weight of the initial specimen, the residual specimen after the removal of a layer and the sliced layer respectively. D_T, D_B and D_R are the density of the total specimen, the residual specimen and the sliced layer respectively. Therefore, the relative density of the removed layer located at a position x_i is

$$\rho_R(x_i) = \frac{D_R(x_i)}{D_M} \quad (D_M \text{ is the matrix density}) \tag{5}$$

and the relative porosity is hence

$$f_R(x_i) = 1 - \rho_R(x_i), \tag{6}$$

where the current location of the layer x_i is updated after each step.

By repeating of the above procedure one can determine the density (or porosity) distribution along one given dimension.

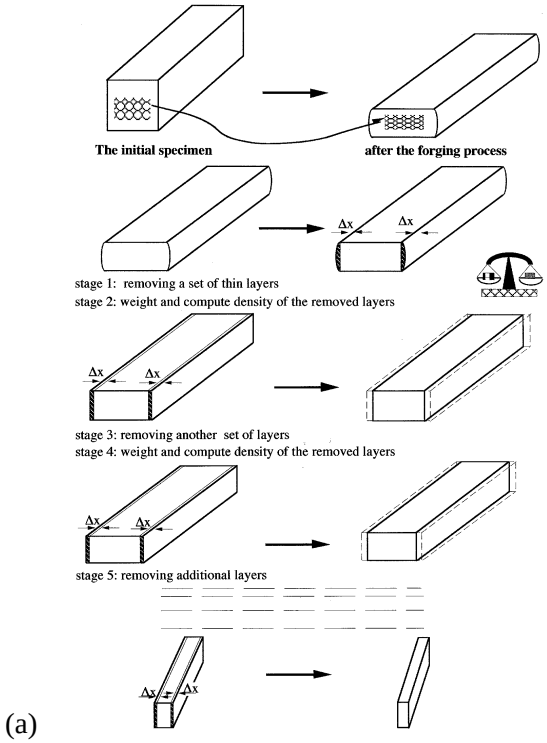

(a)

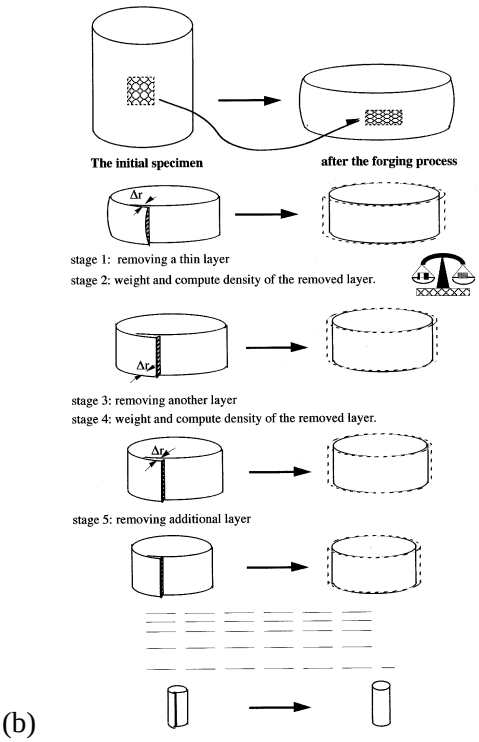

(b)

Figure 3. The various steps of the experimental procedure for macroscopic measurement of the pore distribution: (a) long; (b) circular disk.

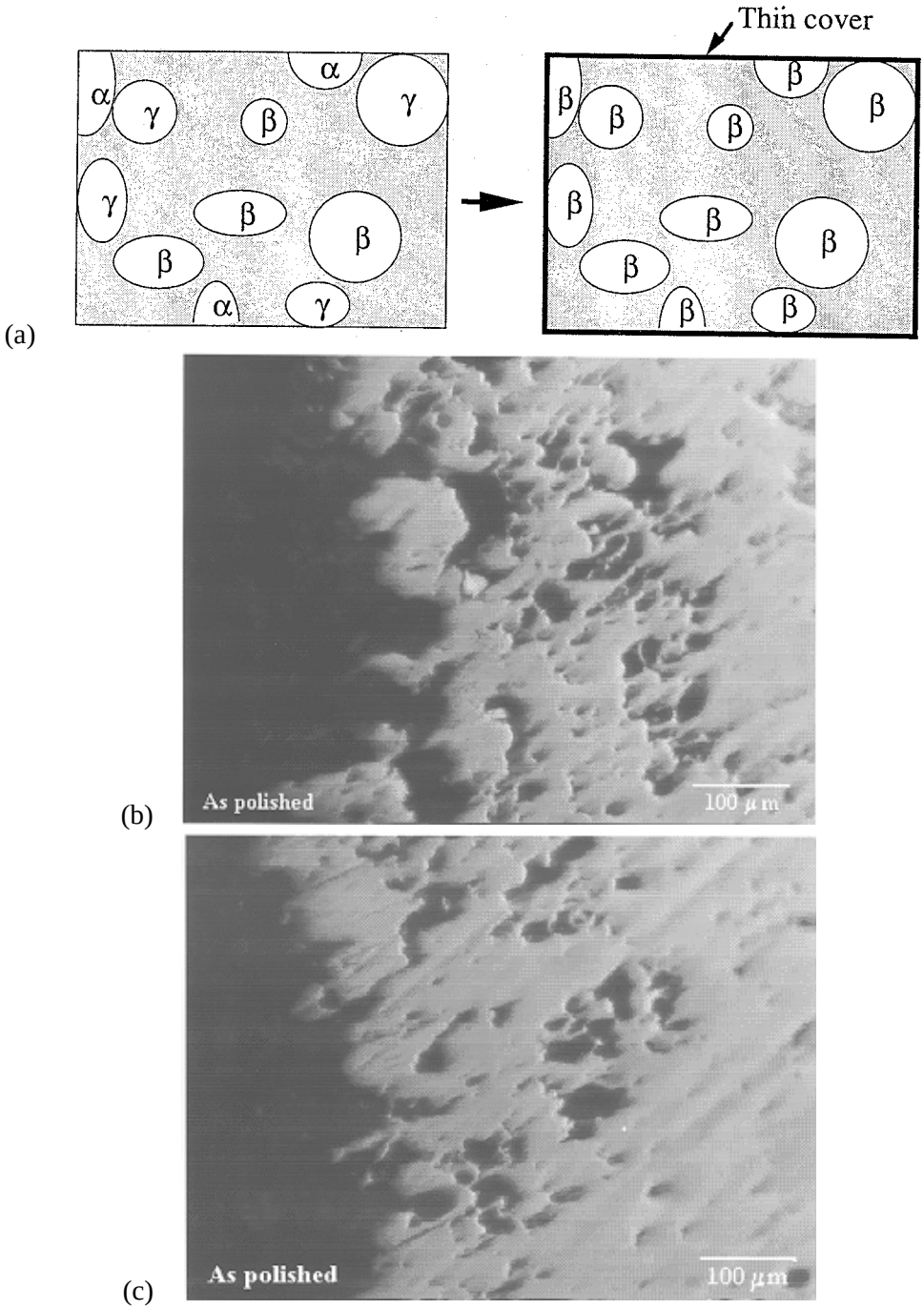

(a)

(b)

(c)

Figure 4. (a) A schematic illustration of cross section in porous material. In general, the material contains open pores (α), closed pores (β) and ill-defined (γ). The thin cover turns all pores into β kind thus decreasing experimental errors; (b) and (c) the free boundary of stainless steel 304 sintered powder specimen (after height reduction of 30 percent). It demonstrates the complexity in measuring accurately the material volume when soaked in distilled water, as required by the standard weighting procedure (ASTM standard, B311-86).

4.2. THE MICROSCOPIC MEASUREMENT

This technique is based on a metallographic characterization of a typical cross section of the workpiece. A characteristic microstructure of selected spots on the cross section is optically enlarged and saved for further digital editing. Then, the area fraction of the dark/bright areas is measured by a computerized scanner. The pores area fraction (which is the ratio of the dark areas to the total area) represents the 2-dimensional porosity distribution in the considered cross section. The precision in assessing pore distribution depends on the number of chosen selected spots and the definition of damage with respect to the gray levels of the pictures. A typical example of damage distribution in Fe structure (in a plain strain specimen that underwent 20 percent height reduction) is shown in Figure 5.

5. Results and discussion

The damage distribution in the upsetting process of the sintered porous specimens was determined using the above mentioned measuring techniques. Two materials were prepared by powder metallurgy techniques: Fe (commercially pure) and stainless steel 304 with initial average relative density of 0.72 and 0.68, respectively. Two different geometries of forged specimens were investigated: parallelepiped, presenting a plane strain condition and axisymmetric disk (Figure 2). The experimental results are compared herewith to a semi-analytical solution (Shirizly et al., 1996) algorithm of which is recapitulated in the Appendix. In these figures (6–10) we used various values of the constants q_1, q_2, q_3 and N. In Figures 6b and 9 (axisymmetric case) the values were selected in accordance with Gurson's criterion (1). In the other figures, the values were chosen on a 'best-fit' basis with the average porosity results.

Figures 6a and 6b exhibit the average density evolution in the specimens as determined by the 'macroscopic method' for both geometries. It is noted that the semi-analytical model reproduces reasonably well the observed trend of the densification process. These figures also show the role of the interfacial tool/material friction in accelerating the overall densification. The shear friction parameter m ($0 < m < 1$) is used to represent the two extremes; the value of $m = 0$ means a frictionless slip between the material and the tools (punch and die), whereas the value of $m = 1$ means the stick slip condition.

We did not attempt to compare the planar and bulk porosity estimation techniques as they provide *complementary* information: the bulk measurement gives an average estimate while planar measurement provides information about the *variations* in planar porosity.

The initial density in 'as is' materials is generally not uniform (see e.g., Schneider, 1996; Becker, 1987). Since our suggested experimental techniques are essentially destructive, the initial distribution of a tested specimen is obviously unknown *a priori*. It may, however, be postulated or estimated based on the measurements of specimen from 'the same batch'. Partially, this is the reason why the pore distributions (shown in Figures 7a , 7b and Figures 8a and 8b along the x-direction) are relatively widely scattered. In any event, the comparison between the experimental scattered data and the analytical predictions of the density distribution is, at least, not inconsistent. The data were collected from tests in plane strain compression with sintered iron, and similarly in Figure 9 for axisymmetric upsetting of stainless steel (SS-304).

For the case described in Figures 7a, 7b we have made the simplifying assumption of an initially uniform density ($\rho_0 = 0.72$) not indicated on these figures to maintain clearness. The subsequent distribution $\rho(x)$ was calculated by the semi-analytical model with and without interfacial friction.

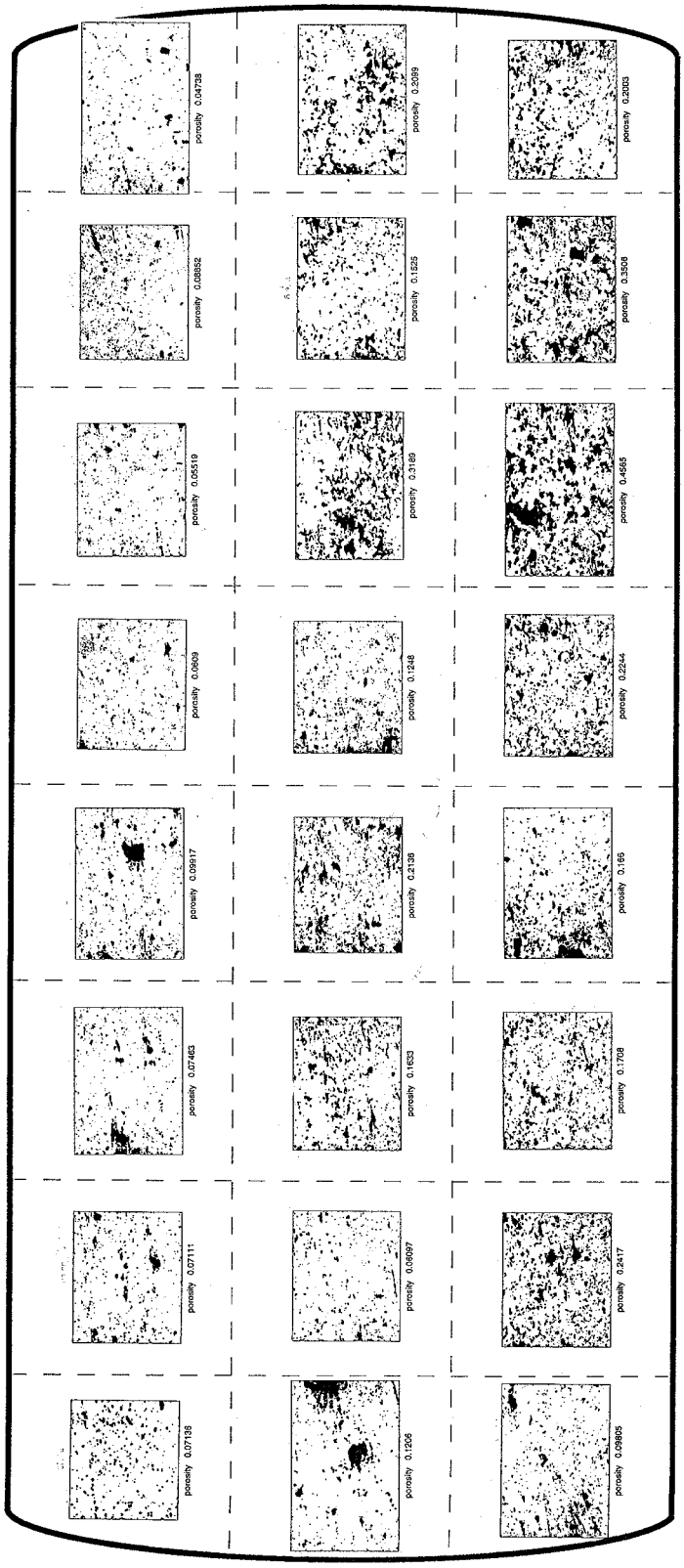

Figure 5. An example of a metallographic characterization of the damage distribution in a Fe specimen made of sintered powder material after 20 percent reduction in height (average initial porosity: 0.28; average terminal porosity 0.16).

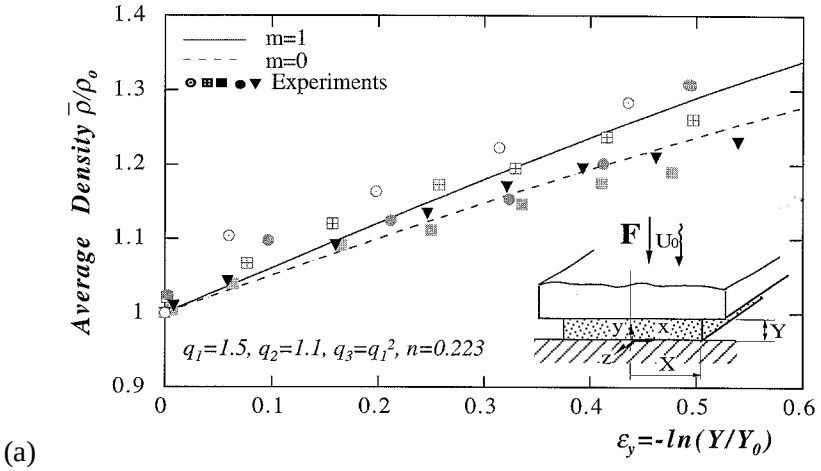

(a)

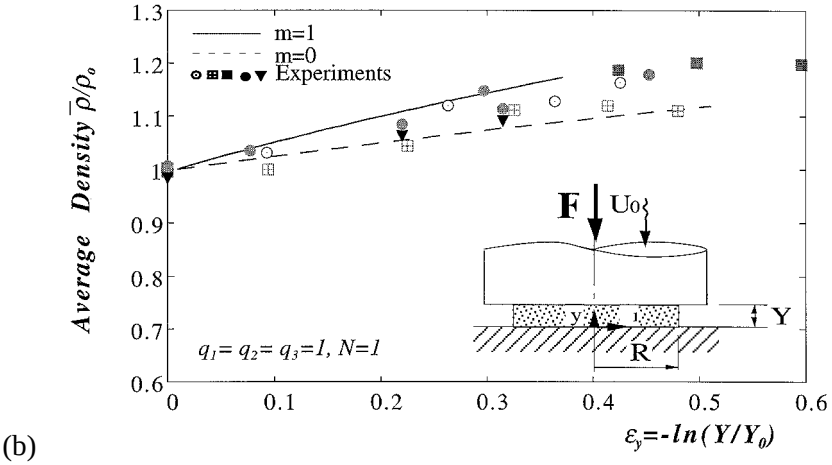

(b)

Figure 6a and 6b. The average density evolution with respect to the reduction of the height of the specimen. Different colors represent different specimens having nearly the same initial porosity. The limit values (0 and 1) of the shear vector 'm' exhibit a frictionless slip and stick slip conditions between the material and the tools, respectively.

The results show the influence of friction on the densification process. For frictionless forming, the density remains uniform whereas frictional conditions cause a distribution of the density throughout the workpiece. Regardless of the forming process, a higher density is anticipated (and observed) at the center of the specimen. Since an initial non-uniform distribution of pores is a reality, it will be studied next.

In Figure 8 a randomly nonuniform initial density distribution is assumed (in the range of 0.72 ± 0.04). By the advancement of the press ($\Delta Y/Y_0 = 0.38$ in Figure 8a and 0.48 in Figure 8b) the density distribution is gradually uniformized. This seems to be somewhat more pronounced if the interfacial friction is minimized ideally to $m = 0$. The main feature in the densification process of having more residual pores near the free edges compare to the center, is repeated consistently.

In assessing the quality of the suggested measuring techniques, it appears that in the initial stage of the unidirectional densification, both measuring techniques yield a similar scattering of the results. When the process progresses, the microscopic technique gives somewhat a

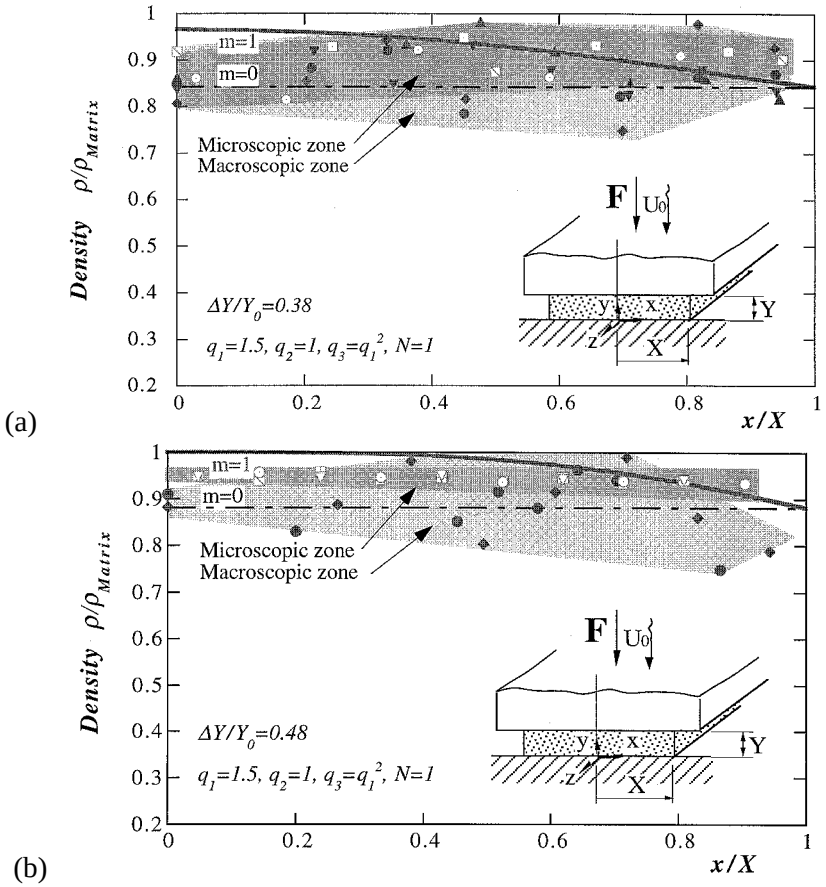

Figure 7a and 7b. Starting from an initial density of $\rho_0 = 0.72$, it is shown that after height reduction of $\Delta Y/Y_0 = 0.38$ (Figure 7a) and $\Delta Y/Y_0 = 0.48$ (Figure 7b) the uniformity is not remained. The theoretical solid curves (simulated a high frictional condition with the tools, $m = 1$) indicate higher residual porosity near the free edge of the workpieces compared to their center (at $x = 0$). In contrast, if the friction is null, $m = 0$, the densification process is progressed uniformly throughout (dashed lines). The different background colors (light green and light yellow) accentuates the zones at which the data is associated with one of the two measurement techniques (the 'macroscopic method' and the 'microscopic method' respectively).

lower scatter than the macroscopic one. This conclusion is based on averaging each data point from three independent tests. As before, the friction retards the uniformization of the density distribution. In all cases, when friction is unavoidable, the zones near the edges of the workpiece are more damaged (by residual pores) than in the center.

The density distribution along the axisymmetric stainless steel disk is shown in Figure 9. A high degree of non uniformity was observed in the initial density of the specimen (0.68 ± 0.11) due to the manufacturing process. In these experiments, the maximum attainable strain was 0.45 (given height reduction of $\Delta Y/Y_0 = 0.36$), beyond which surface cracks appeared.

The measured density is scattered with respect to the analysis, but the analytical predictions fit satisfactorily the trend in the radial distribution of the experiments.

The analytical model also allows to predict the forging force. The evolution of this force vs. stroke for iron forging is shown in Figure 10. The experimental results are well bounded by the analysis when employing the maximum friction ($m = 1$) and the minimal one ($m = 0$). The

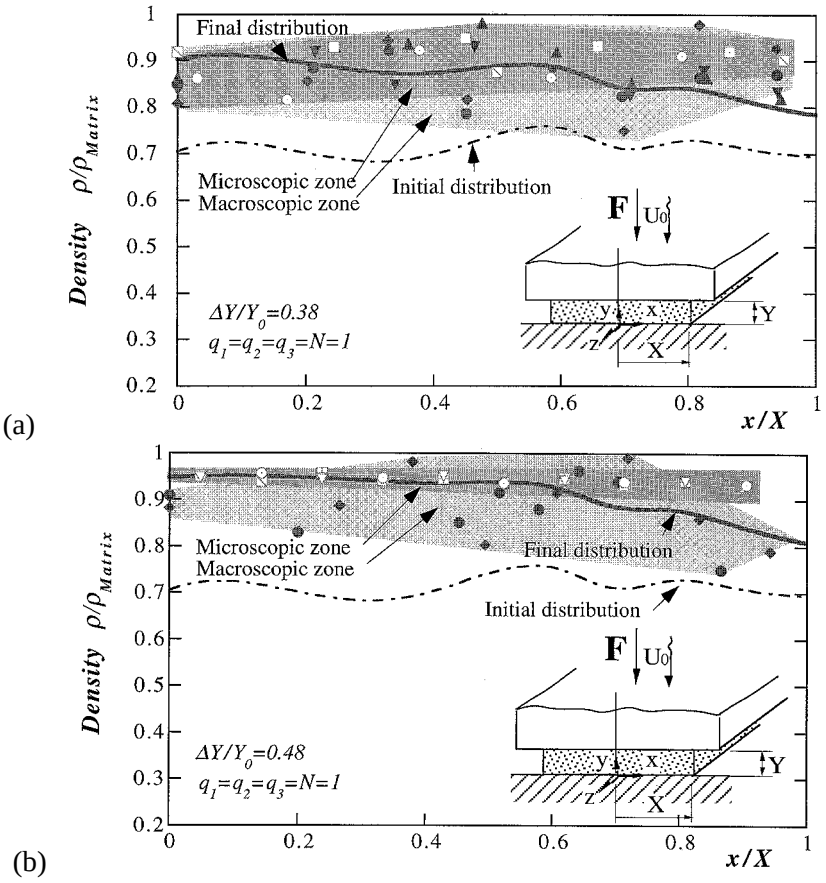

Figure 8a and 8b. Starting from an initial density of $\rho_0 = 0.72$, it is shown that after height reduction of $\Delta Y/Y_0 = 0.38$ (Figure 8a) and $\Delta Y/Y_0 = 0.48$ (Figure 8b) the initial nonuniform distribution is gradually uniformized (shown by dashed-dot lines). The theoretical solid curves (simulated a high frictional condition with the tools, $m = 1$) indicate higher residual porosity near the free edge of the workpieces compared to their center (at $x = 0$). In contrast, if the friction is null, $m = 0$, the densification process is progressed uniformly throughout (dashed lines). The different background colors (light green and light yellow) accentuates the zones at which the data is associated with one of the two measurement techniques (the 'macroscopic method' and the 'microscopic method' respectively).

agreement in predicting the load allows the design of a forging process of porous materials solely on the basis of knowing the material's initial density, matrix flow stress and an estimation of the shear friction coefficient.

Summary

(a) Damage distribution in porous material undergoing unidirectional compression was introduced. This aspect of the forging process has not been addressed in previous analytical work, to our knowledge. This refinement was achieved here by combining a semi-analytical model with experimental observations. Two different experimental techniques for assessing pore distribution were employed and evaluated.

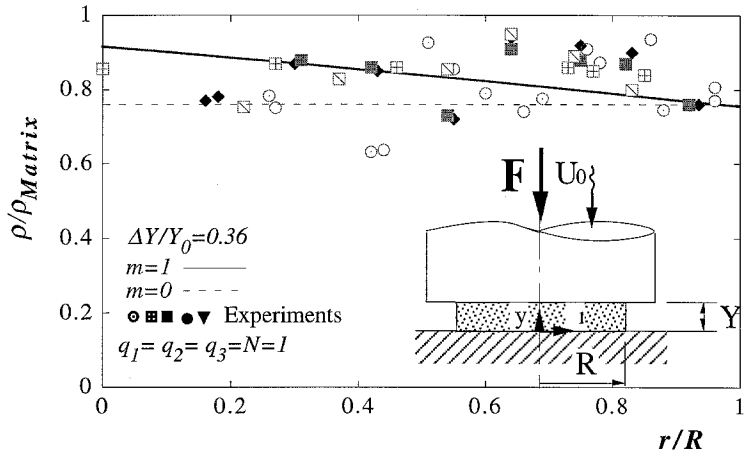

Figure 9. The distribution of the pore density in the radial direction of a regular disc made from sintered stainless steel powder (SS-304). The measurement was done by the 'macroscopic technique' after the disc (initial density of 0.68) was compressed to height reduction of $\Delta Y/Y_0 = 0.36$. The solid line indicates a shear factor of $m = 1$ and the dash line indicates a shear factor of $m = 0$.

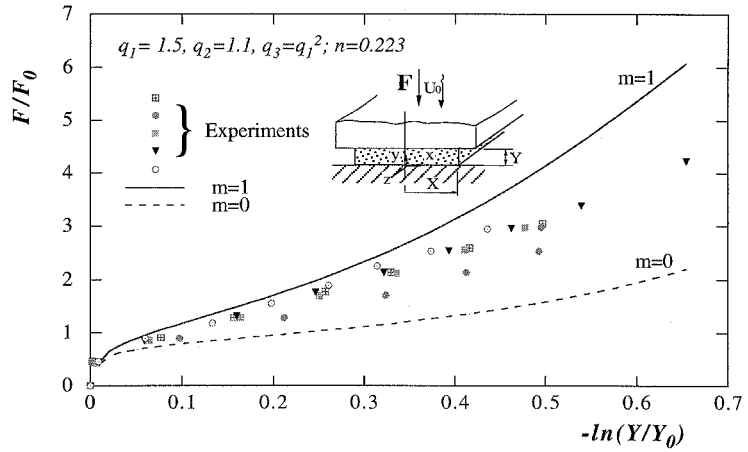

Figure 10. Prediction of the press load during an upsetting process of a long bar made from sintered powder of Fe. It is seen that the experimental results are well bounded by the analysis when employing the extreme friction conditions ($m = 1$ for maximum interfacial shear and $m = 0$ for the minimal one).

(b) The repeatability and the reliability of the suggested methods were tested in two different geometries: parallelepiped specimens (presenting a plane strain condition) and an axisymmetric disks. All tests were done under displacement controlled compression.

(c) Two sintered materials were used: (coomercially pure) iron for testing the parallelepiped specimens and stainless (SS-304) steel for testing the axisymmetric disks.

(d) Results obtained by the two measuring methods are compared satisfactorily with the predictions employing a semi-analytical model (based on the limit analysis approximations).

(e) Interfacial friction along the material/tools surfaces has a considerable influence on the density distribution of the final product. The general tendency is to enhance densification far from the free boundaries. The knowledge that the region near the edges are eventually more porous than the center has a clear implication to the user of the forged product.

Appendix: The basic algorithm

The algorithm for the solution is based on limit analysis approach. In the following Appendix, the outline of the solution is presented for the plain strain case, while with a few variations it can be applied (skipped here) for the axisymmetric case.

(a) *The lower bound solution*
The idea is to devise a statically admissible stress field for the four unknown components:

$$\Sigma_x, \varepsilon_y, \Sigma_z \quad \text{and} \quad \Sigma_{xy}. \tag{A.1}$$

The expressions for the above stresses are reached from the following four conditions:

(i) the condition of plane strain: $D_z^p = 0$; (A.2)
As a result, the stress component Σ_z is

$$\Sigma_z = \tfrac{1}{3}\Sigma_{kk} - \tfrac{1}{9}q_1 q_2 N f^N \bar{\sigma} \sinh\left(q_2 \frac{N}{2}\frac{\Sigma_{kk}}{\bar{\sigma}}\right). \tag{A.3}$$

(ii) The equation of equilibrium in the x-direction (free surface barreling is ignored)

$$\frac{\partial \Sigma_x}{\partial x} = 2\frac{\Sigma_{xy}}{Y}, \tag{A.4}$$

where Σ_{xy} is the shear stress acting on the material/tools interface and the boundary condition for the stress in the x-direction is $\Sigma_x\,(x = X) = 0$.

(iii) The equation of yielding (Equation 1).

(iv) An assumption about the shear stress distribution

$$\Sigma_{xy} = m\bar{\sigma}(1-f)(x^2 - Xx), \tag{A.5}$$

where m is the friction factor, $(0 \leqslant m \leqslant 1)$.

The shear stress of (A.5) is admissible in the sense that it satisfies the stress-free boundary condition

$$\Sigma_{xy}(x = 0) = 0 \quad \text{and} \quad \Sigma_{xy}(x = X) = 0. \tag{A.6}$$

In view of the arbitrary assumption of (iv) the overall results of (A.1) are merely an *admissible stress value* which conforms with a classical lower bound solution.

By having Σ_{kk}, the stress distribution $\Sigma_y(x_i)$ (which is also the traction transmitted to the bar by the punch) is solved. The required punch load (per unit length) is readily obtained as a lower bound (superscripted as 'LB') by integrating the traction along the contact surface as

$$F^{LB} = \int_{-X}^{X} \Sigma_y \, \mathrm{d}x. \tag{A.7}$$

(b) *The upper bound approximation*

In principle, the upper bound approach is based on an energy-rate balance equation whose terms are expressed by an admissible velocity field. The idea is to devise a kinematically admissible velocity field which has to satisfy:

(i) The velocity component u_y satisfies the boundary condition

$$u_y(y=0)=0 \quad \text{and} \quad u_y(y=Y)=-u_0. \tag{A.8}$$

(ii) The condition of plane strain (A.2).

(iii) The compressibility equation

$$D^p_{kk}=\frac{\dot{f}}{1-f}. \tag{A.9}$$

(iv) The kinematic continuity throughout the body $D^p_{ij}=\frac{1}{2}(u_{i,j}+u_{j,i})$. (A.10)

The applied energy rate (Fu_0) should balance the sum of several energy dissipation-rate terms. Here, the dissipation rate terms are those which arise by the plastic deformation of the bulk flow and frictional loss along the interfaces with the tools, $(\dot{W}_{\text{def}}+\dot{W}_f)$ respectively.

The equality in the energy balance yields an upper bound estimation of the load

$$F^{UB}=\frac{\dot{W}_{\text{def}}+\dot{W}_f}{u_0}, \tag{A.11}$$

where the energy rate of the deformation

$$\dot{W}_{\text{def}}=\int_v \frac{\Sigma_{ii}D^p_{jj}}{6}\,\mathrm{d}v+\int_v\left[\left(\frac{\Sigma_{ii}D^p_{jj}}{6}\right)^2+\tfrac{2}{3}H\bar{\sigma}^2D'^p_{ij}D'^p_{ij}\right]^{1/2}\mathrm{d}v, \tag{A.12}$$

when

$$H=[1+q_3f^{2N}]-2q_1f^N\cosh\left(q_2\frac{N}{2}\frac{\Sigma_{kk}}{\bar{\sigma}}\right)+q_1q_2f^N\frac{N}{2}\frac{\Sigma_{kk}}{\bar{\sigma}}\sinh\left(q_2\frac{N}{2}\frac{\Sigma_{kk}}{\bar{\sigma}}\right) \tag{A.13}$$

and rate of energy loss due to friction

$$\dot{W}_f=\int_{S_f}\Sigma_{xy}|\Delta U|\,\mathrm{d}s_f. \tag{A.14}$$

The surfaces s_f on which the integration is performed are the areas along which the plastic flow has a relative slip Δu with the rigid tools.

(c) *Evolution of porosity distribution*

Employing the 'normality rule' on the modified Gurson's yielding function (1), the constitutive equation and the first strain rate invariant are

$$D^p_{ij}(x)=\dot{\Lambda}\left[3\frac{\Sigma'_{ij}(x)}{\bar{\sigma}^2}+\delta_{ij}q_1q_2\frac{N(f(x))^N}{\bar{\sigma}}\sinh\left(q_2\frac{N}{2}\frac{\Sigma_{kk}(x)}{\bar{\sigma}}\right)\right], \tag{A.15}$$

$$D^p_{kk}(x)=3\dot{\Lambda}q_1q_2\frac{N(f(x))^N}{\bar{\sigma}}\sinh\left(q_2\frac{N}{2}\frac{\Sigma_{kk}(x)}{\bar{\sigma}}\right). \tag{A.16}$$

By dividing (A.16) by D_y^p from (A.15), one gets

$$\frac{D_{kk}^p}{D_y^p} = \frac{3q_1q_2Nf^N \sinh\left(q_2\frac{N}{2}\frac{\Sigma_{kk}}{\bar{\sigma}}\right)}{3\frac{\Sigma'_y}{\bar{\sigma}} + \frac{1}{3}q_1q_2Nf^N \sinh\left(q_2\frac{N}{2}\frac{\Sigma_{kk}}{\bar{\sigma}}\right)}. \tag{A.17}$$

Let's define the following

$$\dot{f} = \frac{\mathrm{d}f}{\mathrm{d(time)}}, \qquad D_y^p = \frac{\mathrm{d}\varepsilon_y}{\mathrm{d(time)}}, \qquad \mathrm{d}\varepsilon_y = \frac{\mathrm{d}Y}{Y_0}. \tag{A.18}$$

Substituting the definitions (A.18) and the compressibility Equation (A.9) in the left-hand side of (A.17), replacing the deviatoric stress Σ'_y by the Cauchy stress components, use the plain strain condition (A.2) and the solution of the equilibrium (A.4), one gets the evolution equation

$$\frac{\mathrm{d}f}{\mathrm{d}\varepsilon_y} = \frac{3q_1q_2Nf^N(1-f)\sinh\left(q_2\frac{N}{2}\frac{\Sigma_{kk}}{\bar{\sigma}}\right)}{\frac{\Sigma_{kk}}{\bar{\sigma}} - \frac{6}{\bar{\sigma}Y}\int_X^x \tau(\xi)\,\mathrm{d}\xi + \frac{2}{3}q_1q_2Nf^N \sinh\left(q_2\frac{N}{2}\frac{\Sigma_{kk}}{\bar{\sigma}}\right)}, \tag{A.19}$$

where $\tau(\xi)$ is the shear friction function given in (A.5) (frictional shear model $\tau(x) = \Sigma_{xy}(x)$ at $y = y(0, Y)$ should be known *a priori*).

Acknowledgments

The work was supported by the Niedersachsen Fund, with the cooperation of Hannover University Group (in Hannover, Germany), headed by Prof. E. Doege. The authors are thankful to J.W. Ullman Center for Manufacturing Systems & Robotics Research (CMSR) and to the Materials Mechanics Laboratory, both in the Faculty of Mechanical Engineering at Technion.

References

ASTM Standard B311-86. *Standard Test Method For Density Of Cemented Carbides*.

Becker, R. (1987). The effect of porosity distribution on ductile failure. *Journal of the Mechanics and Physics of Solids* **35**, 577–599.

Gurson, A.L. (1977). Continuum theory of ductile rapture by void nucleation and growth: part I – Yield criteria and flow rules for porous ductile media. *Transactions of ASME, Journal of Materials and Technology* **99**, 2–15.

Haghi, M. and Anand, L. (1993). A constitutive model for isotropic, porous, elastic-viscoplastic metals. *Mechanics of Materials* **3**, 37–53.

Moon, J.H. and Yang, D.Y. (1992). A method of measurement for determination of relative density in axisymmetric forming of sintered porous material. *Journal of Materials Processing Technology* **33**, 311–318.

Schneider, G., Postler, I. and Wuhrl, I. (1996). Quantitative structure analysis with sintered materials. *Structure* **29**, 19–23.

Shirizly, A., Tirosh, J. and Rubinski, L. (1996). *On the Densification Process of Porous Materials Under Uniaxial Compression: Theory and Experiments*. Submitted.

Spitzig, W.A., Kelly, J.F. and Richmond, O. (1985). Quantitative characterization of second-phase populations. *Metallography* **18**, 235–261.

Spitzig, W.E., Smelser, R.E. and Richmond, O. (1988). The evolution of damage and fracture in iron compacts with various initial porosities. *Acta Metallurgica* **36**, 1201–1211.

Tirosh, J. and Iddan, D. (1989). Forming analysis of porous materials. *International Journal of Mechanical Science* **31**, 945–965.

Tvergaard, V. (1981). Influence of voids on shear band instabilities under plane strain conditions. *International Journal of Fracture* **17**, 389–407.

Tvergaard, V. (1982). On localization in ductile materials containing spherical voids. *International Journal of Fracture* **18**, 237–251.

Wang, P.T. and Karabin, M.E. (1990). Evolution of porosity during thin plate rolling of porous metals. *Microstructural Evolution in Metal Processing, ASME PED* **46**, 47–58.

Wang, P.T. and Richmond, O. (1992). Overview of a two state variable constitutive model for the consolidation and forming processes of powder-based porous metals. *Mechanics of Granular Materials and Powder Systems, ASME MD* **37**, 63–81.

Wray, P.J., Richmond, O. and Morrison, H.L. (1983). Use of the Dirichlet tessellation for characterizing and modeling nonregular dispersions of second-phase particles. *Metallography* **16**, 39–58.